



**HAL**  
open science

# Neural computation analysis of alumina-titania wear resistance coating

Sofiane Guessasma, Mokhtar Bounazef, Philippe Nardin

► **To cite this version:**

Sofiane Guessasma, Mokhtar Bounazef, Philippe Nardin. Neural computation analysis of alumina-titania wear resistance coating. *International Journal of Refractory Metals and Hard Materials*, 2006, 24 (3), pp.240-246. 10.1016/j.ijrmhm.2005.05.012 . hal-00159354

**HAL Id: hal-00159354**

**<https://hal.science/hal-00159354>**

Submitted on 16 Jul 2024

**HAL** is a multi-disciplinary open access archive for the deposit and dissemination of scientific research documents, whether they are published or not. The documents may come from teaching and research institutions in France or abroad, or from public or private research centers.

L'archive ouverte pluridisciplinaire **HAL**, est destinée au dépôt et à la diffusion de documents scientifiques de niveau recherche, publiés ou non, émanant des établissements d'enseignement et de recherche français ou étrangers, des laboratoires publics ou privés.

# Neural computation analysis of alumina–titania wear resistance coating

Sofiane Guessasma <sup>a,\*</sup>, Mokhtar Bounazef <sup>b</sup>, Philippe Nardin <sup>c</sup>

<sup>a</sup> LERMPS, Université de Technologie de Belfort-Montbéliard (UTBM), Site de Sévenans, 90 010 Belfort Cedex, France

<sup>b</sup> Hydrology and Materials Laboratory, Sidi Bel Abbe's University, Algeria

<sup>c</sup> FEMTO ST, UMR CNRS 6174- CREST, Parc Tech., Belfort, France

Pin-on-disc tests were performed on alumina–13 wt.% titania coatings obtained under several APS conditions. Friction coefficient data were analysed using artificial neural network. This permitted to predict parameter ranges for which good wear resistance is possible when varying each of the process parameters individually with respect to a reference condition. In this case, results suggest that large parameter ranges did not permit to obtain a significant friction coefficient variation which was mainly between 0.51 and 0.61. In addition, injection parameters and total plasma gas flow rate were the control factors.

*Keywords:* Artificial neural network; Alumina–titania coating; Atmospheric plasma spraying; Wear resistance; Friction coefficient

## 1. Introduction

Thermal spraying is a technique of coating manufacturing implementing a wide variety of processes and materials. The atmospheric plasma spraying (APS) is one of these processes based on the creation of a plasma jet to melt a feedstock powder. Powder particles are injected with the aid of a carrier gas and gain their velocity and temperature by thermal and momentum transfers from the plasma jet. At the surface of the substrate, such particles flatten and solidify rapidly forming a stacking of lamellas. Coating microstructure is then characterized by a heterogeneous phase configuration with porosity content due to the voids left by the stacking process. Microcracks appear also in the microstructure as a consequence of stress accommodation due to high spray temperature and a large difference in thermal expansion

coefficients between substrate and coating. This is mainly the case of ceramic coatings deposited on metallic substrates.

Plasma sprayed alumina–titania ceramic is one of the materials largely used in APS process. It is known for its wear, corrosion and erosion resistance applications.

The control of the ceramic in-service properties and especially the wear behaviour is sensitive to the large number of the processing parameters and their inter-dependencies [1]. Such control is obviously complex to establish and most models consider a fewer number of control factors having direct correlations with the processing parameters. In this paper, wear resistance of alumina–titania coatings is analysed by varying APS process parameters. These were selected based on their main effects on particle velocity and temperature before substrate impingement and thermal stresses through spray temperature increase. Analysis based on artificial neural network [2] was conducted in order to predict the coupled effects between arc current and other process parameters. Laser profilometry was used to assess

\* Corresponding author. Tel.: +33 3 84 21 43 89; fax: +33 3 84 58 32 86.

E-mail address: sofiane.guessasma@utbm.fr (S. Guessasma).

the wear track profiles and improve the knowledge of the wear mechanisms and its relationship with the microstructure thermally sprayed coatings.

## 2. Experimental procedure

### 2.1. Coating fabrication

Alumina–13 wt.% titania ceramic powder (METCO 130) was thermally sprayed onto metallic coupons ( $\varnothing 25 \text{ mm} \times 10 \text{ mm}$ ) under atmospheric plasma spraying conditions. The elongated shape of the powder particles facilitates the heat transfer from the plasma jet required to melt the particles (Fig. 1a). However, this morphology is not the best one for the injection of such particles in the plasma jet because of the lower “flowability”.

Five process parameters were varied, namely arc current ( $I$ ), hydrogen fraction ( $H/A$ ), total plasma gas flow rate ( $H + A$ ), carrier gas flow rate (CG) and injector

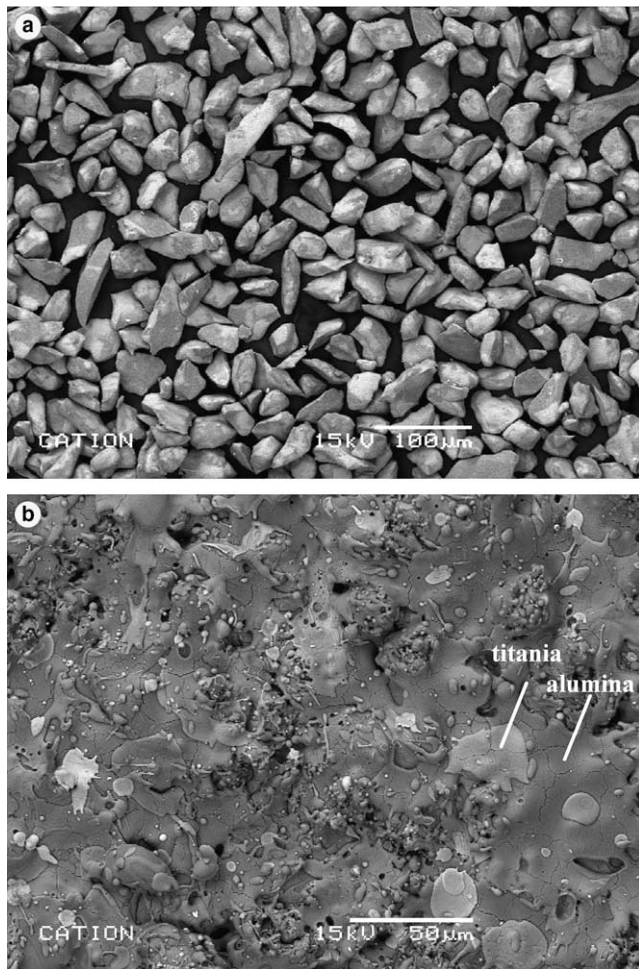


Fig. 1. (a) Morphology of the alumina–titania powder particles. (b) A top view of the microstructure of alumina–titania coating revealed using SEM microscopy.

Table 1  
Experimental layout

	Value
<i>Spray parameter</i>	
Gun	Sulzer-Metco F4
Feedstock feed rate	22 g min <sup>-1</sup>
Spray distance	125 mm
Spray angle	90°
Scanning step	12 mm
Cooling air jets	2
Scanning velocity	16 mm s <sup>-1</sup>
<i>Pin-on-disk test</i>	
Sliding velocity	0.33 m s <sup>-1</sup>
Applied load	5 N
Sliding distance	1000 m

diameter (ID). The three first parameters are known to influence significantly the plasma jet properties (enthalpy, velocity, etc.) and the last ones influence particle trajectories in the plasma jet. The other process parameters were fixed to reference values as shown in Table 1. The microstructure of alumina–titania coatings presents common features to ceramic coatings processed using thermal spraying (Fig. 1b). These features are porosities, splat configuration and microcracks which form due to the low thermal expansion coefficient of the ceramic material which accommodate the stresses in the coatings.

Wear tests were performed using a pin-on-disc (POD) arrangement (Fig. 2) on a CSEM<sup>1</sup> tribometer (single point contact). The coated sample was slid against a 6 mm ball made of WC/Co under an applied load of 5 N. The sliding contact was maintained at 8 mm from the sample centre. The sample was rotated at 394 rpm corresponding to a linear speed of 0.33 m s<sup>-1</sup>. The sliding distance was approximately 1000 m. Wear test parameters are shown also in Table 1.

### 2.2. Artificial neural network concept

Experimental data were analysed using artificial neural network methodology [2,3]. Such concept is a robust statistical technique which learns from experimental data by training process and relates between inputs and output of a given problem [4]. In this study, the inputs were the arc current, hydrogen fraction, total plasma gas flow rate, carrier gas flow rate and injector diameter. The output is the friction coefficient. Neurons act as mathematical processing units and permit to transform the input values and transmit them to the output in a way that the predicted response approaches the experimental one. Each neuron is characterised by an

<sup>1</sup> CSEM: Centre Suisse d’Electronique et de Microtechnique SA, Jaquet Droz 1, 2007 Neuchâtel, Switzerland.

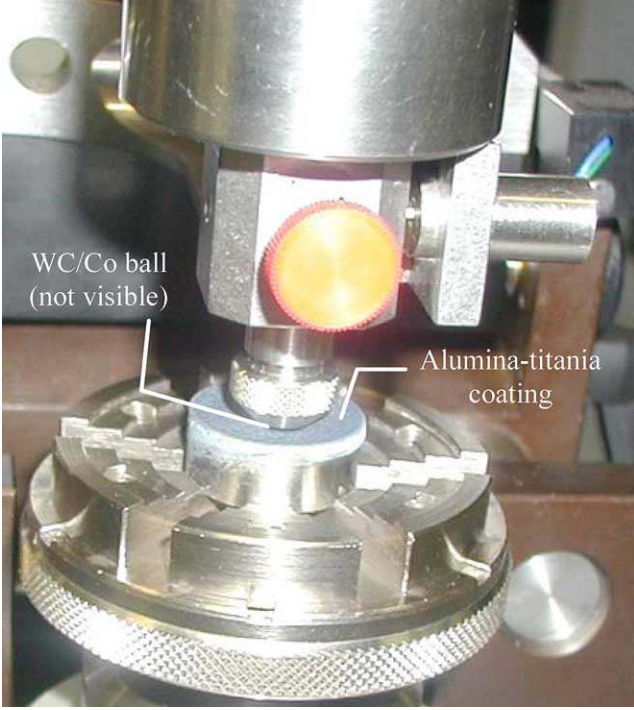


Fig. 2. POD disc arrangement.

input, an output and an activation function and these are related in the following form

$$O(x_i) = f[I(x_i)] \quad (1)$$

where  $O(x_i)$  is the output of neuron  $x_i$ ,  $f$  is the transfer or activation function which transforms nonlinearly the neuron input  $I(x_i)$  of neuron  $x_i$ . In this study, the sigmoid function was used as a transfer function.

Neurons are connected with means of numbers called weights. Each neuron receives the weighted sum from the other neurons, following the relationship

$$I(x_i) = w(x_i, y_j)O(y_j) = O(x_i, y), \quad j = 1, N_y \quad (2)$$

where  $w(x_i, y_j)$  represents the weight value between neuron  $x_i$  and  $y_j$  from layers  $x$  and  $y$ , respectively.  $N_y$  represents the number of the neurons in the layer  $y$  connected to neuron  $x_i$ .

The optimization process of the neural network consists in adjusting the weight values in way to lower the difference between the predicted and the real responses. The calculation starts by zeroing the weights and calculating the quadratic error of the network output

$$w(x_i, y_j) = 0 \quad \forall i \text{ and } j \quad (3)$$

$$J^t = \frac{1}{2} (\vec{r}_0 - \vec{r}_t)^2 \quad (4)$$

where  $r_t$  is the predicted response of the neural network at the iteration level  $t$ ,  $r_0$  is the true response issued from the database.  $k$  represents the index of the neurons in the output layer  $z$ .

Weights are corrected according to the quick propagation algorithm

$$\Delta w(x_i, y_j)^t = \frac{\nabla J_y(x_i, y_j)^t}{\nabla J_y(x_i, y_j)^{t-1} - \nabla J_y(x_i, y_j)^t} \times \Delta w(x_i, y_j)^{t-1} \quad (5)$$

where  $\Delta w^t$  is the weight change at the iteration level  $t$ . The max iteration level is 1000 cycles for any run.  $\Delta J$  represents the error rate.

The number of neurons in the network is a part of the optimisation process and is selected based on the minimum residual error for each run (Fig. 3). The maximum neuron number allowed in the structure is calculated for a weight number lower than 1.5 times the database size. A database of 16 cases (Table 2) enlarged 10 times was used to obtain the optimized structure, using the following equation

$$(O_k, I_k)_{\text{new}} = (O_k, I_k)_{\text{original}} + \text{GAUSS}() * (\delta_{O_k}, \delta_{I_k}) \quad (6)$$

where  $(O_k, I_k)_{\text{original}}$  and  $(O_k, I_k)_{\text{new}}$  are the  $k$ th set of input and output patterns in the original and enlarged databases. GAUSS() is a random number generator from a Gaussian distribution of numbers between  $-1$  and  $1$ . The couple  $(\delta_{O_k}, \delta_{I_k})$  represents the standard deviation associated to the experimental results.

The database enlargement permits to tune a large number of weight parameters and is known as a ‘‘jitter effect’’ in the ANN formalism [5,6]. An optimized

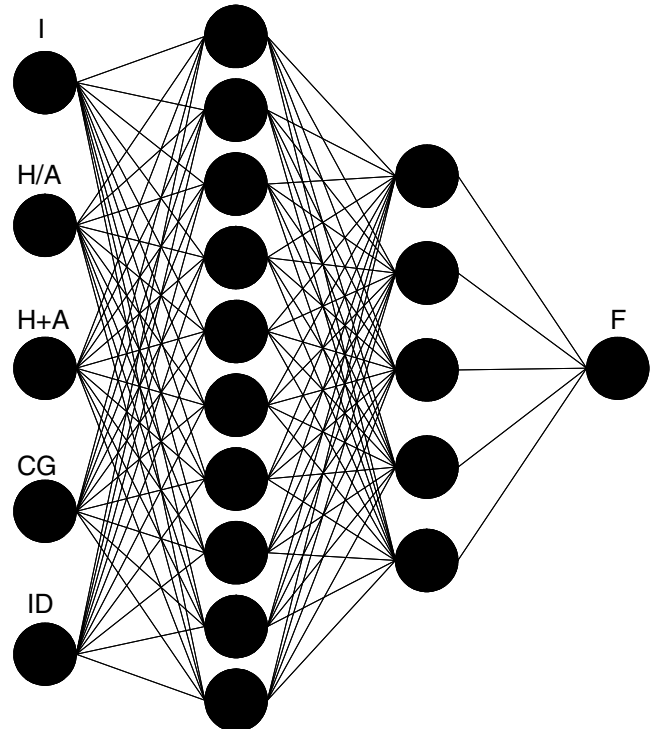


Fig. 3. Optimized artificial neural network architecture.

Table 2

Experimental and predicted friction coefficient values for the considered tests

Exp	I	H/A	A + H	CG	ID	F	
						Experimental	Predicted
C1	440	35	30	2.6	1.5	0.578 ± 0.010	0.587 ± 0.009
C2	440	35	30	3.7	1.8	0.523 ± 0.011	0.531 ± 0.009
C3	440	35	60	2.6	1.8	0.548 ± 0.012	0.550 ± 0.001
C4	440	35	60	3.7	1.5	0.533 ± 0.010	0.537 ± 0.004
C5	440	13	40	2.6	1.8	0.532 ± 0.011	0.544 ± 0.012
C6	440	13	40	3.7	1.5	0.591 ± 0.012	0.596 ± 0.005
C7	440	43	40	2.6	1.5	0.557 ± 0.012	0.569 ± 0.012
C8	440	43	40	3.7	1.8	0.521 ± 0.011	0.527 ± 0.005
C9	630	35	30	2.6	1.8	0.562 ± 0.011	0.569 ± 0.007
C10	630	35	30	3.7	1.5	0.563 ± 0.010	0.572 ± 0.009
C11	630	35	60	2.6	1.5	0.536 ± 0.010	0.541 ± 0.006
C12	630	35	60	3.7	1.8	0.551 ± 0.012	0.558 ± 0.007
C13	630	13	40	2.6	1.5	0.545 ± 0.011	0.553 ± 0.008
C14	630	13	40	3.7	1.8	0.527 ± 0.010	0.532 ± 0.004
C15	630	43	40	2.6	1.8	0.574 ± 0.012	0.578 ± 0.004
C16	630	43	40	3.7	1.5	0.542 ± 0.011	0.547 ± 0.006

structure (Fig. 3) related process parameters to friction coefficient value.

### 3. Results and discussion

#### 3.1. Surface finishing and wear behaviour

The relationship between roughness of the slid materials is an important factor which determine the nature of the wear process. In ceramic materials especially alumina based materials, the wear can be identified as a combination of several mechanisms including tribochemical reaction, plastic flow, plowing and microfracture. The formation of the tribofilm is dependent on these mechanisms and mainly influenced by the roughness of the part and the counter parts during the plowing process. When sliding the WC/Co ball presenting a high surface finishing state against none-grounded coatings, it was remarked that negative wear operates (Fig. 4). This is identified as the deposition of the ball material on the coating surface as shown in Fig. 4b. Samples which were ground before performing the wear tests presented positive wear (Fig. 5). In addition, large roughness causes significant vibrations of the magnetic sensor in the POD arrangement which can false the estimation of the friction coefficient.

#### 3.2. Process parameters and friction coefficient

Experimental friction coefficient values obtained from POD tests were analysed using the cumulative normal probability plot [7]. This method permitted to obtain mean friction coefficient value and related standard deviation associated to the steady-state regime (Fig. 6). In this case, scatter around mean values did

not exceed 3% and represented friction coefficient fluctuation during sliding. Predicted friction coefficients obtained using neural computation exhibited a low scatter related to experimental values. This was less than 2.2%. In Table 2, this scatter is expressed as function of the experimental values as the absolute difference between the experimental and predicted responses.

Fig. 7 shows the predicted evolution of friction coefficient with respect to process parameters. These are expressed in a non-dimensional form, which writes

$$y = \frac{x - x_{\min}}{x_{\max} - x_{\min}} \quad (7)$$

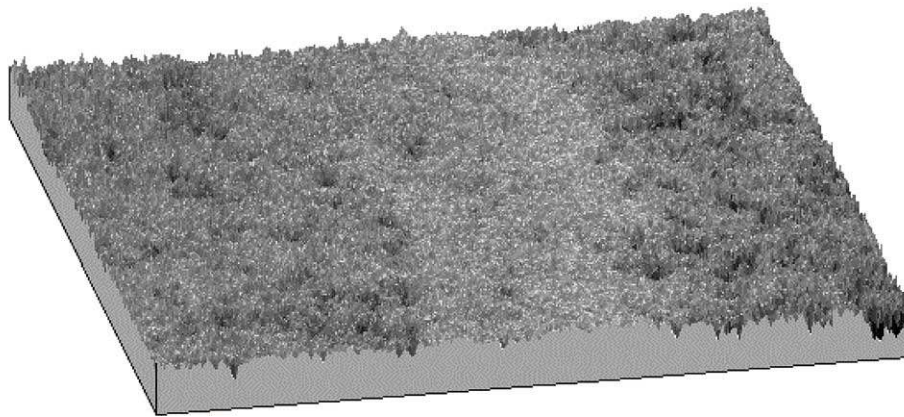
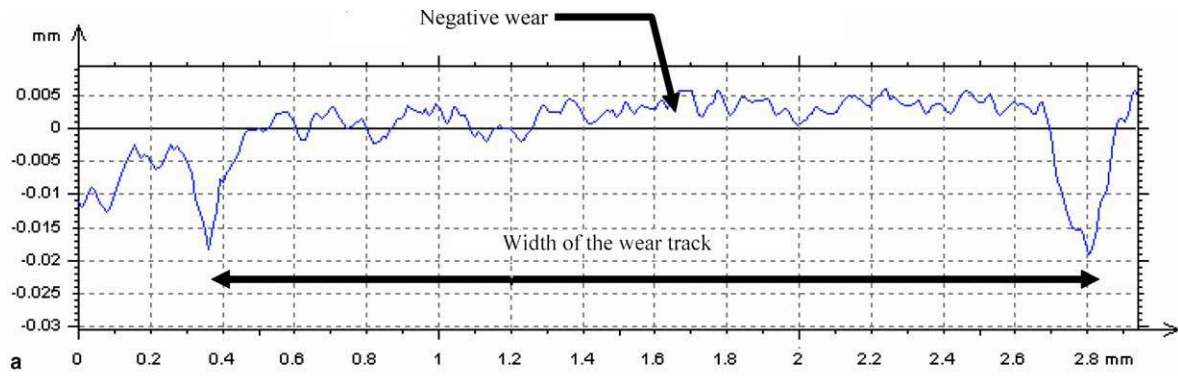
where  $y$  is the formatted value relative to parameter value  $x$ , max and min values associated to parameter  $x$  are summarized in Table 3. The  $x_{\min}$  and  $x_{\max}$  values represent the process window for which the main influence of any variable is correctly represented. When the variable range is scanned in the dimensionless form, the sensitivity to the friction coefficient is rendered equivalent to any variable and thus the influences can be measured properly.

Predicted results are obtained by varying individually process parameters at the input of the network and keeping the others to a reference condition. Fig. 7 shows that friction coefficient decreases with all process parameter increase. This suggests that reference condition is not an optimized thermal spray condition. Friction coefficient was more sensitive to injection parameters, namely carrier gas flow rate and injector diameter and total plasma gas flow rate. Table 3 gives the friction coefficient relative increase with respect to individual process parameter variations. The range for each variable was selected larger than the experimental range to show the predictive way of the neural network. In this range, the most admitted values in the process window are represented. This is calculated assuming the following relationship

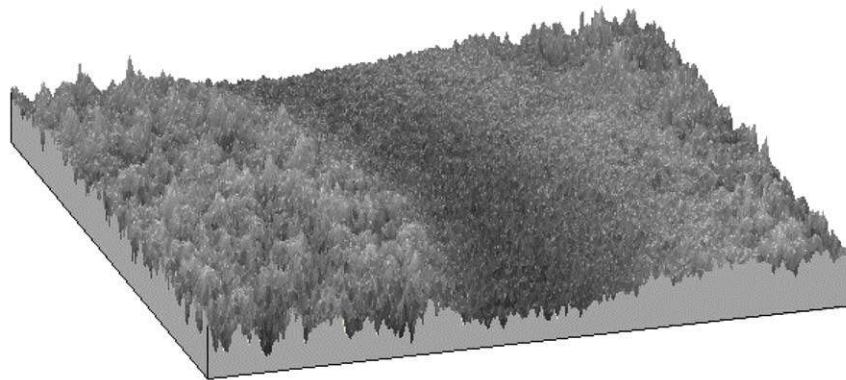
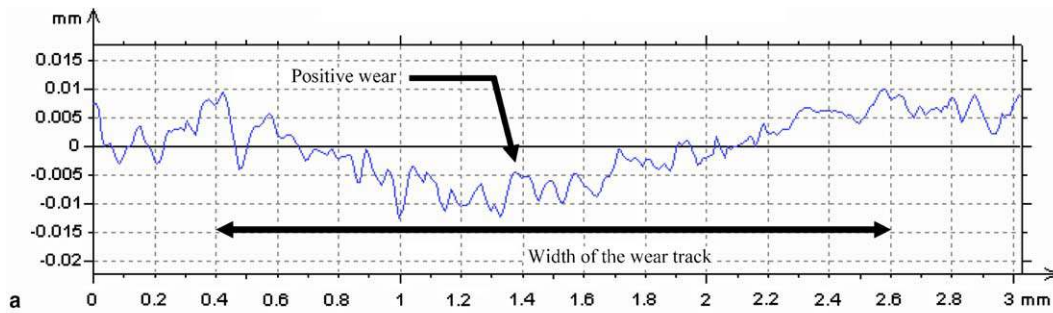
$$r(\%) = 100 * \frac{F_{\max}(y) - F_{\min}(y)}{F_{\min}(y)} \quad (8)$$

where  $r$  is the relative variation corresponding to parameter efficiency.  $F_{\max}$  and  $F_{\min}$  are maximum and minimum friction coefficient values obtained when varying process parameter  $y$ .

The role of arc current can be explained by an effect on the available energy for powder particle heating and acceleration before substrate impingement [8]. An increase of the plasma energy with the increase of arc current improves flattening process of particles as their viscosity and surface tension decrease. This in turn reduces porosity level between lamellas [9] and increases inter-lamellar cohesion [10]. Cohesion improvement is responsible for a good wear resistance and can explain the decrease of friction coefficient. However, the low



**b**  
 Fig. 4. Wear track showing negative wear analysed used laser profilometry. (a) Elevation profile and (b) 3D surface roughness map.



**b**  
 Fig. 5. Wear track showing positive wear analysed used laser profilometry. (a) Elevation profile and (b) 3D surface roughness map.

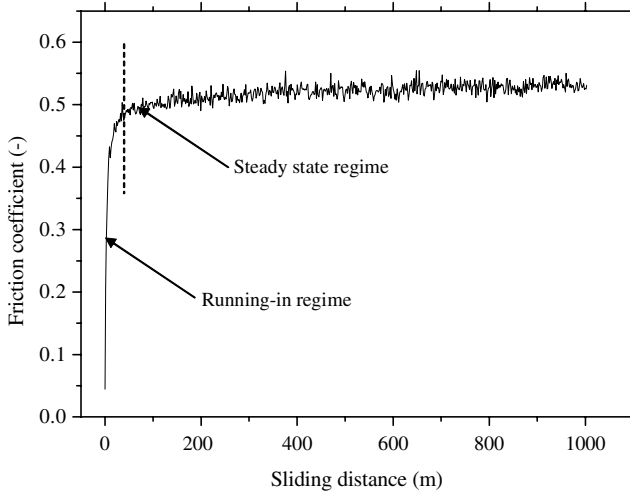


Fig. 6. Typical POD curve showing the evolution of friction coefficient with respect to sliding distance.

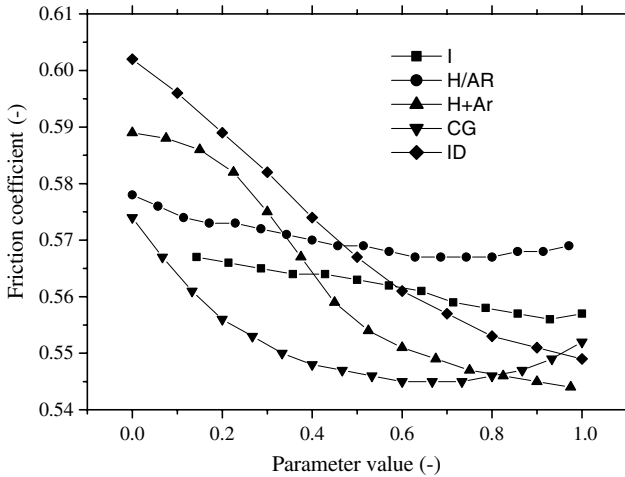


Fig. 7. Friction coefficient variation as function of process parameters keeping at each time the other parameter at a reference value. (ref.:  $I = 440$  A;  $H/A = 35\%$ ;  $H + A = 40$  SLPM;  $CG = 2.6$  SLPM;  $ID = 1.5$  mm).

Table 3  
Friction coefficient relative variation with respect to process parameters

Parameter type (unit)	$I$ (A)	$H/A$ (%)	$H + A$ (SLPM)	$CG$ (SLPM)	$ID$ (mm)
Parameter range, $x_{min}-x_{max}$	400–680	10–45	25–65	2.5–4	1–2
Friction coefficient relative variation (%)	2	2	8	5	10

decrease of friction coefficient, which is within the standard deviation, indicates that injection parameters were not adapted, especially carrier gas flow rate. Indeed, this parameter controls particle injection velocity. When the

flow rate is too low, initial particle velocity is not sufficient to overcome plasma jet viscosity. In the counter part, if carrier gas flow rate is too high, particles may cross the plasma jet and degrade consequently coating properties. Thus, the dependence of friction coefficient on carrier gas flow rate can be approximated by a parabolic curve for which an optimal should exist. Despite of the fact that there is only two experimental sets available to show the influence of this parameter, the neural net learnt the correlations based on the whole enlarged database. Thus, the decrease of friction coefficient relative to the increase of this parameter can be explained by an improved particle trajectory in the plasma jet [11] which increases particle temperature.

A large injector diameter seems to be more adequate and can be related to an increased particle velocity dispersion [8]. Its influence is more correlated to spray temperature rather than to particle velocity and temperature. Indeed, energetic parameters increase microcrack density in the microstructure by the increase of coating temperature because of the increase of the heat flux transmitted to the workpiece and different thermal expansion coefficients between ceramic coating and metallic substrate. Microcrack density is expected to be lower when varying injection parameters especially injector diameter.

Hydrogen ratio plays the same effect as arc current because it improves plasma jet enthalpy and viscosity [12]. However, this parameter did not exhibit a significant effect on friction coefficient. This can be explained by the low arc current value associated to hydrogen variation. When the hydrogen ratio is sufficient, plasma energy level associated to total plasma gas flow rate becomes more important and plays thus the same role as that of arc current. However, the increase of argon gas in the mixture decreases particle temperature because of plasma core shortening associated to a more diffuse plasma [9,12]. In this case, particle injection must be adapted in order to introduce particles deeply in the plasma jet [8]. This can explain the sigmoid shape associated to total plasma flow rate increase.

### 3.3. Microstructure and friction coefficient

The discussion of process parameter effects can be reduced to the discussion to the available energy to melt particles. The analysis of the particle temperature profiles during their flight towards the substrate shows clearly the shift of the temperature distribution when increasing the net energy (Fig. 8a). A lower condition set would have the consequence to lower the coating cohesion and to provoke the incursion of unmolten particles (Fig. 8b). These can increase the plowing phenomenon before the formation of the glassy film and increases the friction coefficient.

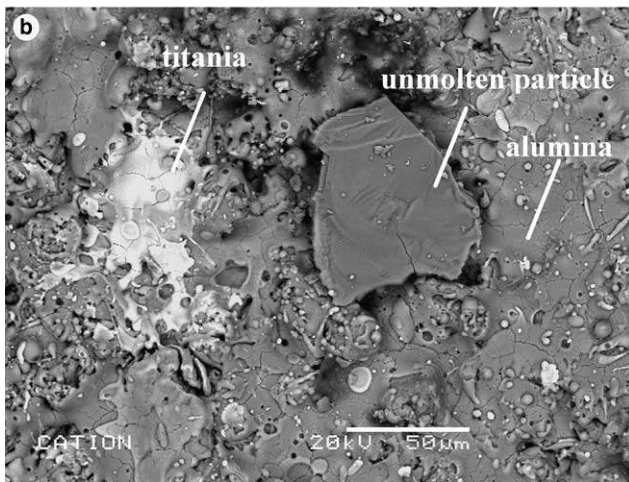
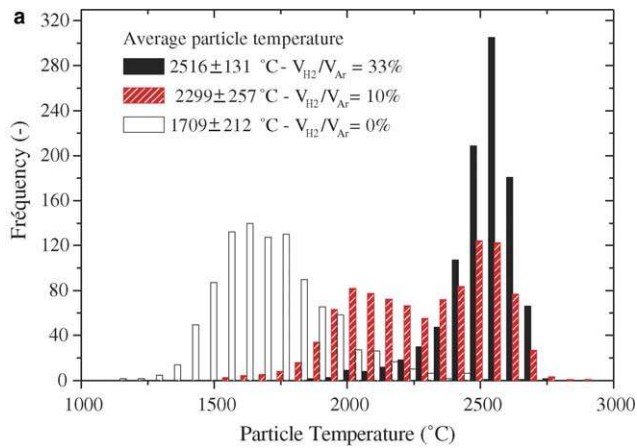


Fig. 8. (a) Temperature distribution of powder particles during thermal spraying recorded using bichromatic analyser. Increase of hydrogen ratio in the plasma jet increases the energy of the plasma jet and consequently particle temperature before impingement into the substrate. (b) A top view of alumina-titania coating showing the splashing of particles and the incursion of unmolten particles due to a small available energy in the plasma jet.

#### 4. Conclusions

Friction coefficient of alumina–13 wt.% titania exhibited a low variation with respect to process parameters. This variation was predicted to be less than 10% when using an artificial neural network. All process parameters, when varied individually with respect to a reference condition, improved wear resistance. This study pointed out the role of injection parameters and total plasma gas flow rate in the control of friction coefficient evolution. Arc current and hydrogen ratio were not efficient

parameters when considering their relative increase with respect to the reference condition. In order to study other process parameter combinations at the input of the artificial neural network, a methodology is under development based on hypervolume representations in order to predict optimal parameter ranges for which wear resistance is improved.

#### Acknowledgement

LERMPS is a member of the Institut des Traitements de Surface de Franche-Comté (ITSFC, surface treatment institute of Franche-Comté), France.

#### References

- [1] Pawlowski L. The science and engineering of thermal spray coatings. John Wiley & Sons; 1995.
- [2] Guessasma S. PhD thesis, UTBM, Belfort, France, no 006, 2003.
- [3] Guessasma S, Montavon G, Coddet C. On the neural network concept to describe the thermal spray deposition process: An introduction. Proceedings of 3rd international thermal spray conference, 2002 international thermal spray conference and exposition. Düsseldorf, Germany: DVS-Verlag GmbH; 2002. p. 435–9.
- [4] Guessasma S, Montavon G, Coddet C. Modeling of the APS plasma spray process using artificial neural networks: Basis, requirements and an example. *Comput Mater Sci* 2004;29(3): 315–33.
- [5] Holmstrom L, Koistinen P. *IEEE Trans Neural Net* 1992;3: 24–38.
- [6] An G. The effect of introducing noise during backpropagation training on a generalization performance. *Neural Comput* 1996;8:643–74.
- [7] Li J, Liao H, Coddet C. Friction and wear behavior of flame-sprayed PEEK coatings. *Wear* 2002;252:824–31.
- [8] Fauchais P, Vardelle M. Plasma spray processes: Diagnostics and control. *Pure Appl Chem* 1999;71:1909–18.
- [9] Friis M, Persson C, Wigren J. Influence of particle in-flight characteristics on the microstructure of atmospheric plasma sprayed yttria stabilized ZrO<sub>2</sub>. *Surface Coat Technol* 2001; 141:115–27.
- [10] Varacalle DJ, Herman H, Bancke GA, Riggs WL. Vacuum plasma sprayed alumina–titania coatings. *Surface Coat Technol* 1992;54/55:19–24.
- [11] Zhang T, Gawne DT, Liu B. Computer modelling of the influence of process parameters on the heating and acceleration of particles during plasma spraying. *Surface Coat Technol* 2000;132:233–43.
- [12] Prystay M, Gougeon P, Moreau C. Structure of plasma sprayed zirconia coatings tailored by controlling the temperature and velocity of the sprayed particles. *J Therm Spray Technol* 2001;10:67–75.